



**Abstract**

The shape of ice-shelf cavities are a major source of uncertainty in understanding ice-ocean interactions. This limits assessments of the response of the Antarctic ice sheets to climate change. Here we use vibroseis seismic reflection surveys to map the bathymetry beneath the Ekström Ice Shelf, Dronning Maud Land. The new bathymetry reveals an inland-sloping trough, reaching depths of 1100 m below sea level, near the current grounding line, which we attribute to erosion by palaeo-ice streams. The trough does not cross-cut the outer parts of the continental shelf. Conductivity-temperature-depth profiles within the ice-shelf cavity reveal the presence of cold water at shallower depths and tidal mixing at the ice-shelf margins. It is unknown if warm water can access the trough. The new bathymetry is thought to be representative of many ice shelves in Dronning Maud Land, which together regulate the ice loss from a substantial area of East Antarctica.

**Plain Language Summary**

Antarctica is surrounded by floating ice shelves, which play a crucial role in regulating the flow of ice from the continent into the oceans. The ice shelves are susceptible to melting from warm ocean waters beneath them. In order to better understand the melting, knowledge of the shape and depth of the ocean cavity beneath ice shelves is crucial. In this study we present new measurements of the sea floor depth beneath Ekström Ice Shelf in East Antarctica. The measurements reveal a much deeper sea floor than previously known. We discuss the implications of this for providing routes for warm ocean waters to melt the base of the ice shelf, and discuss how the observed sea-floor features were formed by historical ice flow regimes. Although Ekström Ice Shelf is relatively small, the geometry described here is thought to be representative of the topography beneath many ice shelves in this region, which together regulate the ice loss from a substantial area of East Antarctica.

**1 Introduction**

Ice shelves surrounding Antarctica act as buttresses, restraining ice discharge from the continent into the oceans, and therefore regulating Antarctic contributions to sea-level rise (Dupont & Alley, 2005). Mass loss from Antarctica has been accelerating over the past 20 years (IPCC, 2019), driven by increased basal melting of ice shelves (Paolo et al., 2015; Pritchard et al., 2012). Accurate knowledge of the geometry of the ice-shelf

54 cavities and the properties of the water column beneath them are essential for under-  
55 standing processes active at the ice-shelf ocean interface. Recent studies have highlighted  
56 a lack of sub-ice shelf bathymetry as a “major limitation” (Pattyn et al., 2017) for fu-  
57 ture projections of Antarctic mass balance. Improved bathymetric mapping allows de-  
58 termination of water access pathways and calculation of spatially and temporally vari-  
59 able melt rates (e.g. Cochran et al., 2014; Goldberg et al., 2019; Milillo et al., 2019; Morlighem  
60 et al., 2020; Tinto et al., 2019; Pattyn et al., 2017). In addition, sub-ice shelf bathymetry  
61 also provides information about ice-dynamic history. Understanding the past ice dynam-  
62 ics and implementing an accurate bathymetry in ice-flow and oceanographic models is  
63 a critical step to improve projections of the evolution of the ice sheets.

64 The coast of Dronning Maud Land (DML), East Antarctica (Fig.1) is fringed by  
65 numerous small ice shelves. In this area, satellite-derived melt rates are typically low (Rignot  
66 et al., 2013). However, the continental shelf is narrow (Fig.1b), meaning the ice shelves  
67 of DML are in close proximity to Warm Deep Water (WDW) masses which flow along  
68 the continental slope, making this a potentially sensitive region to future change (Hattermann,  
69 2018; Heywood et al., 2013; Thompson et al., 2018). It has also been highlighted as sus-  
70 ceptible to marine ice sheet instability (Morlighem et al., 2020; Ritz et al., 2015). In ad-  
71 dition, the ice shelf-ocean interactions along the DML coast play an important role in  
72 preconditioning the structure and water-mass properties of the westward flowing bound-  
73 ary current (Fahrbach et al., 1994; Hattermann, 2018). This current is a key control on  
74 warm-water inflow toward the Filchner-Ronne Ice Shelf (Hellmer et al., 2017; Timmer-  
75 mann & Hellmer, 2013) and bottom water formation in the Southern Weddell Sea (Meijers  
76 et al., 2016; Meredith et al., 2011). The few bathymetric measurements that exist un-  
77 der DML ice shelves have revealed cavities that are much deeper than those included in  
78 current gridded data sets of Antarctica (e.g. Fretwell et al., 2013; Morlighem et al., 2020).  
79 Under the Fimbul Ice Shelf (Fig.1b), a deep trough within the sub-shelf cavity was dis-  
80 covered (Nøst, 2004) and confirmed to contain modified WDW (Hattermann et al., 2012,  
81 2014). At the front of the Roi Baudouin Ice Shelf, in Eastern DML, an 850 m deep trough  
82 is present, which has major consequences when simulating ice-sheet advance and retreat  
83 (Berger, 2017; Favier et al., 2016). This emerging picture highlights the need for more  
84 accurate bathymetry measurements in this region.

85 The general lack of bathymetry measurements beneath ice shelves is the result of  
86 difficulties in access: radar systems, do not penetrate through the water column; grav-

87 ity inversions are possible, but without control points are sensitive to assumptions about  
88 the underlying geology (Eisermann et al., 2020); drilling through the ice provides lim-  
89 ited spatial range and is logistically challenging; and the use of autonomous underwa-  
90 ter vehicles is rare, as they require ship support (e.g. Jenkins et al., 2010; Nicholls et al.,  
91 2006). Seismic surveys currently provide the most reliable method to map water-column  
92 thickness, as well as to image the sea bed below.

93 Here we address this problem using a specialised vibroseis seismic source and snow  
94 streamer system (Eisen et al., 2015) to create a new map of the ice-shelf cavity and sea-  
95 floor bathymetry beneath the Ekström Ice Shelf, DML. Ekström Ice Shelf (Fig.1) cov-  
96 ers an area of approximately 6800 km<sup>2</sup> with basal melt rates of up to 1.1 ma<sup>-1</sup> (Neckel  
97 et al., 2012). It is laterally constrained by the grounded ice rises of Søråsen to the west  
98 and Halvfarryggen in the east (Fig. 1c). The present ice-shelf front is less than 20 km  
99 from the continental shelf break. Until now, little was known about the bottom topog-  
100 raphy of the ice-shelf cavity. A number of seismic reflection measurements by Kobarg  
101 (1988), suggest a southward deepening of the seafloor with a maximum water-column  
102 thickness of 500 m. However, a map of the cavity is currently lacking. We integrate our  
103 bathymetric mapping with conductivity-temperature-depth (CTD) data acquired through  
104 hot-water drilled access holes in the ice shelf and under sea ice in Atka Bay (Fig. 1c).  
105 The combined observations are used to identify the primary implications of this new bathymetry  
106 for ice-ocean interaction and ice-dynamic history in the region. They show the urgent  
107 need for more measurements of sub-ice-shelf bathymetry along the coast of this sector  
108 of Antarctica and for many other ice shelves, where the bathymetry is equally poorly con-  
109 strained.

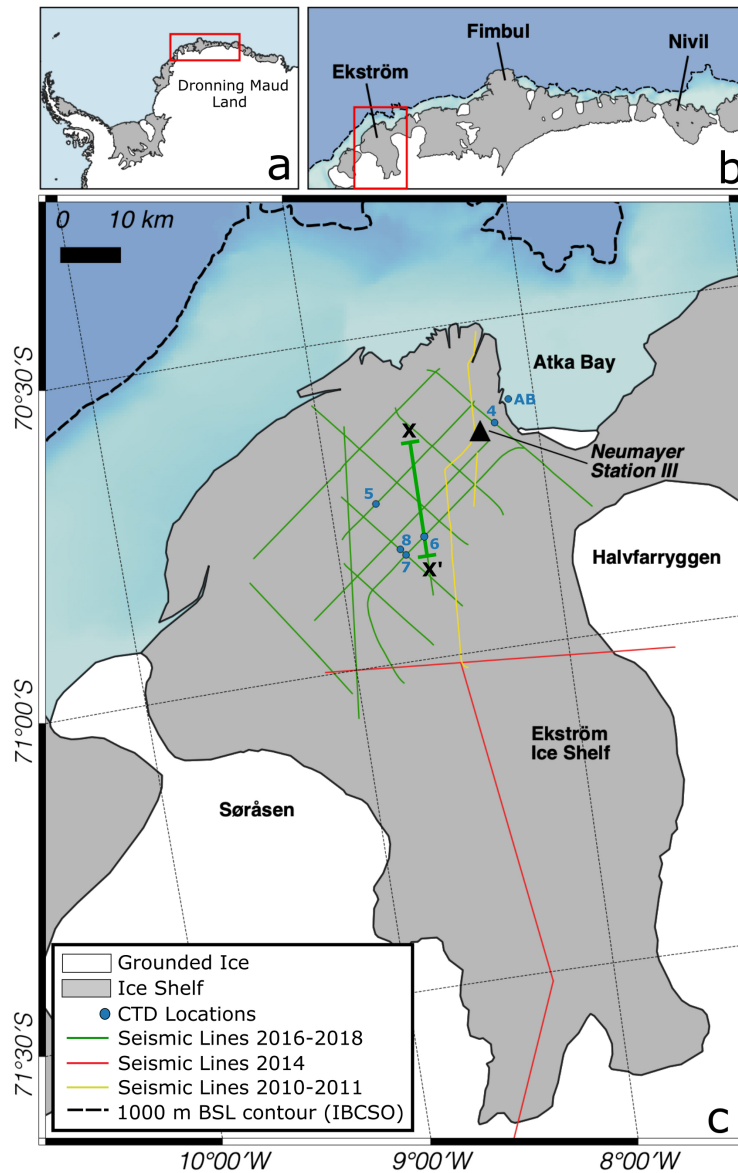


**Figure 1.** a) Location of Dronning Maud Land within Antarctica b) Area highlighted in (a) with location of Ekström Ice Shelf indicated and c) Ekström Ice Shelf with seismic survey lines and CTD locations shown. In all figures the ice shelf is shown in grey and grounded ice in white. In (b) and (c) the ocean background is from the International Bathymetric Chart of the Southern Ocean (IBCSO) (J. E. Arndt et al., 2013), with the 1000 m below sea level (BSL) contour shown as a dashed line, indicating the location of the continental slope. The CTD location labels, ‘4’ to ‘8’ refer to hot-water drilled access holes ‘EIS-4’ to ‘EIS-8’, and ‘AB’ to the location of a sea-ice lead in Atka Bay. The location of the seismic line shown in Fig. 2 is X-X’.

## 2 Data and Methods

### 2.1 Seismic Data Acquisition

Seismic data were collected between 2010 and 2018, using two different vibroseis seismic sources. The snow streamer, used for all data acquisition, was 1500 m long, containing 60 channels, with a 25 m group spacing. Each group contained eight gimbaled P-wave SM-4, 14 Hz geophones. For all data collection the vibroseis source was towed behind a snow tractor with the snow streamer towed behind that. This method of operation allowed for data acquisition rates of up to 20 km per day for 10 fold data. Fold refers to the amount of times a sub-surface point (referred to as a common mid-point or CMP) is sampled by different source/receiver pairs. A more detailed explanation of both these seismic sources, the snow streamer, and the operational method is given in Eisen et al. (2015).

The main grid of data, at the ice shelf front, was collected during the 2016/17 and 2017/18 austral summers (Fig.1c, green) as part of the Sub-EIS-Obs project (Kuhn & Gaedicke, 2015). The seismic source was the AWI IVI EnviroVibe, producing a 10 second linear sweep from 10-220 Hz. These data are relatively high fold (6-15), with the exception of the two lines in the north-western corner of the grid, which are single fold. It was not possible to extend data collection further west due to surface crevassing. The seismic lines extending across the grounding line to the east and south were collected in 2014 (Fig.1c, red), using the same acquisition configuration, and are single fold. Three older lines from 2010 and 2011 overlap the main grid (Fig.1c, yellow) and were acquired using the University of Bergen Failing Y-1100 vibroseis source (Kristoffersen et al., 2014), with a 10 second sweep from 10-100 Hz; fold varies between 1 and 8.

All seismic data were processed specifically for this study, to ensure consistent treatment of data from different surveys (supporting information S1). The resulting seismic time-stacked sections all have clear ice base and the sea floor reflections (Fig. 2). The two-way traveltimes (TWTs) of these reflections were hand-picked on each section.

### 2.2 Depth Conversion and Gridding of Seismic Measurements

The hand-picked TWTs from all seismic lines were used to create grids of the TWT to the ice base and sea floor, using a kriging algorithm. Any mis-ties between picks, in

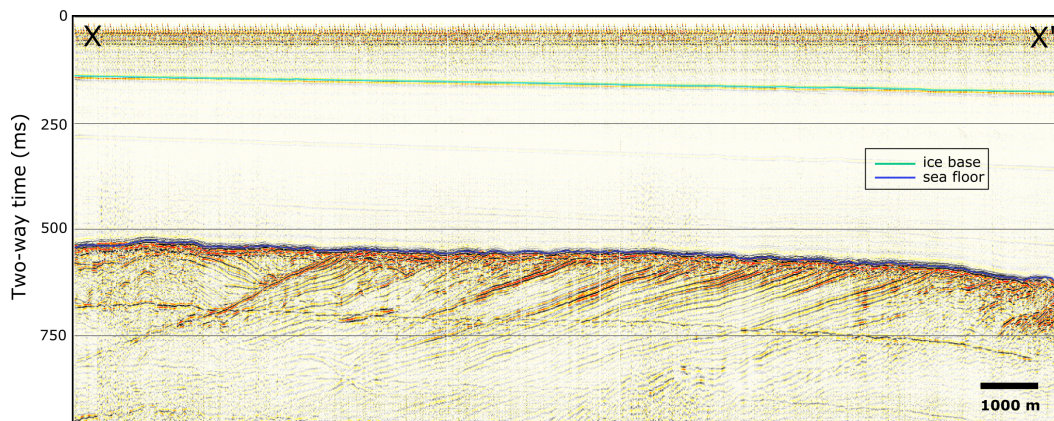


**Figure 2.** Example of a seismic time-stacked section. Location of section is marked X-X' on Fig. 1, AWI line number 20170561. Reflections from the ice-shelf base and sea floor are clearly visible, and the TWT to them can be easily determined. The section is vertically exaggerated by a factor of 10.

140 areas where seismic lines overlap, were handled by assigning priority to the higher res-  
 141 olution surveys. Each grid was then depth converted using a seismic velocity of  $3601 \text{ ms}^{-1}$   
 142 for the ice shelf and  $1451 \text{ ms}^{-1}$  for the water column (supporting information S2). The  
 143 final step was to correct the depth of each grid for the ice surface elevation, using the  
 144 REMA digital elevation model v1.1 (Howat et al., 2019), which was re-referenced to the  
 145 GL04C geoid (Förste et al., 2008).

### 146 2.3 Uncertainties in Seismic Depths

147 Uncertainties in the sea-floor depth, from seismic measurements, come from four  
 148 main sources: (i) accuracy of the horizon picking, (ii) velocities used for depth conver-  
 149 sion of these horizons, (iii) errors in the REMA DEM used for surface elevation correc-  
 150 tions and (iv) depth errors from unmigrated data. A detailed analysis of these individ-  
 151 ual error sources was made (supporting information S3), resulting in cumulative error  
 152 at the sea floor of  $\pm 14.8 \text{ m}$  in the area of the main data grid and  $\pm 34.4 \text{ m}$  in the ar-  
 153 eas of the 2014 seismic lines, which extend from the main grid towards the grounding  
 154 lines (Fig. 1). The gridded bathymetry may have larger errors away from the seismic lines.

155 It was possible to measure the ice thickness and sea-floor depth at the five hot-water  
156 drilled access hole locations (4-8; Fig. 1) on the ice shelf, both during drilling and with  
157 camera equipment and coring devices deployed through the holes to the sea floor. These  
158 measurements confirmed that the seismic determined ice thickness was within  $\pm 5$  m of  
159 the measured thickness and the sea floor within  $\pm 10$ -20 m. This validates our error es-  
160 timates, as the latter range also includes horizontal displacement of the sampling rope  
161 by ocean currents.

## 162 **2.4 CTD Data**

163 During the 2018/19 austral summer, hot-water drilled access holes were made at  
164 five locations on the ice shelf (4-8; Fig. 1). An RBR Concerto CTD sensor was repeat-  
165 edly lowered through each hole and additionally through a sea-ice lead in Atka Bay (AB;  
166 Fig. 1), giving a total of 6 CTD measurement sites. The CTD sensor recorded water mass  
167 properties at a frequency of 1 Hz (vertical resolution of 0.5 - 2 m), from which pressure,  
168 in-situ temperature, and practical salinity data were extracted (see supporting informa-  
169 tion S4). The uncertainty for in-situ temperature is  $0.02^{\circ}\text{C}$  and for practical salinity 0.03.  
170 These data were used to calculate seismic velocities for depth conversion of the sea-floor  
171 seismic reflection (supporting information S2), and to investigate water masses present  
172 beneath the ice shelf and sea ice.

### 3 Results and Discussion

The new sub-ice shelf bathymetry (Fig. 3a) is independent of any previously available products of ice thickness and water depth. Here, we compare the new bathymetry to the Bedmap2 (Fretwell et al., 2013) Antarctic bed topography (Fig. 3b), which has been the baseline Antarctic dataset for the large majority of modelling studies. We highlight the differences to emphasise the need for dedicated measurements of sub-ice shelf bathymetry.

Given the lack of previously available data, the Bedmap2 (Fretwell et al., 2013) sea-floor bathymetry beneath Ekström Ice Shelf closely follows the ice-base topography, deepening towards the grounding line. This suggesting a relatively thin, uniform water-column height of the ice shelf cavity (Fig. 3b). The new seismic bathymetry, in contrast, reveals a much more distinct geometry of the ice shelf cavity (Fig. 3c). Similar mismatches have been documented for other ice shelves in this sector (e.g. Nøst, 2004).

Beneath the main grid of our data (Fig. 3a) we find a bathymetric trough under the central part of the ice shelf, which appears to be aligned with the current ice-flow direction. In this area the trough is 30 km wide and reaches depths of up to 800 m below sea level (Figs. 3a and 3c, C-C'). The trough flanks have depths around 450-500 m (Figs. 3a and 3c, C-C' and D-D'), shallowing to around 300 m depth at the marginal grounding line joining the ice shelf to the ice rise of Halvfarryggen (Figs. 3a and 3c, B-B'). Shallowing topography is also seen towards the western grounding line at Søråsen and it is likely this mirrors the cavity shape to the east. The sea floor directly in front of the ice shelf is 450 m deep, similar to the flanks of the trough. A basin-like depression, around 570 m deep, is seen on the eastern plateau, to the south of Neumayer Station III. The profile from the front of the ice-shelf edge to the current grounding line (Figs. 3a and 3c, A-A'), follows the axis of the trough under the main grid and the single seismic line connecting the south of the grid to the grounding line. This indicates an inland-sloping sea floor (Figs. 3a and 3c, A-A'), reaching a maximum depth of 1100 m around 10 km seaward of the current grounding line.



**Figure 3.** **a)** Gridded sea-floor bathymetry beneath the Ekström Ice Shelf, derived from seismic measurements (this study). **b)** The same area as (a) but with sub-ice shelf bathymetry from Bedmap2 (Fretwell et al., 2013) co-located with the seismic bathymetry. In both (a) and (b) bathymetry seawards of the ice-shelf edge is from the IBCSO (J. E. Arndt et al., 2013) mapping project and is cut to the area where measurements are present, note that ice shelf front was further landward than present day when some measurements were made. White contours are at 50 m intervals. Features I-IV are indicated (see text for details). Grey dashed lines show the seismic data locations, with the cross sections shown in (c) indicated by black dashed lines. Blue points indicate the location of CTD measurements, as in Fig. 1. **c)** Cross sections of the ice-shelf cavity and sea floor beneath and in front of Ekström Ice Shelf. Ice flow direction is indicated by arrows and cross-hairs. Sea-floor bathymetry (brown) is from the seismic grid merged with IBSCO, seaward of the ice-shelf edge. The ice shelf (grey) is derived from gridded seismic data at the ice base and REMA surface elevation. Solid black outlines are areas where data is present, dashed lines in A-A' and D-D' are data gaps. Bedmap2 elevations are shown as brown dashed lines for comparison. All data are referenced to the GL04C geoid.

### 3.1 Ice-Dynamic History

The sea-floor bathymetry under Ekström Ice Shelf allows us to interpret features associated with past ice sheet configurations in this region. The deepened trough under the centre of the ice shelf (Fig. 3a) is interpreted as a relict landscape, formed through erosion by former ice streams. The flanks of the trough and the sea floor at the ice-shelf front are around 300-400 m shallower than the trough. The trough does not cross-cut the outer parts of continental shelf and it is therefore likely that the seaward rising continental shelf was a previous grounding line.

Sediment core records in front of Ekström Ice Shelf are sparse (Grobe & Mackensen, 1992; Hillenbrand et al., 2014) and do not provide conclusive evidence as to whether grounded ice covered the entire continental shelf, as far as the continental slope (approximately the 1000 m contour in Fig. 1), during the Last Glacial Maximum (LGM: 23 - 19 ka BP). Sediment cores from the continental shelf, in front of Ekström Ice Shelf, were not deep enough to penetrate into material from the LGM. The recovered Holocene aged sediments (11.7 ka BP to present), were likely deposited beneath an ice shelf (Grobe & Mackensen, 1992), close to the grounding line. Our finding that the trough does not cross-cut the outer parts of continental shelf suggests that grounded ice likely reached to the inner parts of the continental shelf (around the current ice-shelf front) in the past, possibly at the LGM, but the precise grounding line position remains unresolved.

The seismic line extending from the main grid to the south (Fig. 3c, A-A') shows a sea floor that deepens towards the current grounding line. The general trend of a retrograde slope within the trough would likely have put this area at risk of rapid ice retreat after the LGM, until a stable grounding line position (e.g a topographic high) was reached. There are a number of topographic highs along the ice-flow direction. Particularly prominent is the topographic high at 100 km along profile A-A' (I; Fig. 3c), which is around 200 m above the surrounding sea floor. We suggest that this is a former grounding line position, given its significant elevation. However, current bathymetry measurements in this region do not extend laterally to confirm the extent of this feature. There is a significant overdeepening upstream of this high (II; Fig. 3c), reaching 1100 m depth around 10 km seaward of the current grounding line. Overdeepenings are commonly formed in areas of convergent ice stream flow, where ice velocities and erosional potential are high (Patton et al., 2016). The location of this overdeepening is at the convergence of

233 two tributary glaciers, with higher modern-day ice flow velocities than the surrounding  
234 ice (Neckel et al., 2012). When ice was thicker and grounded further seaward, the overdeep-  
235 ened area would have been at the junction between these two tributaries, eroding the  
236 deep basin. Overdeepenings typically terminate in sills (Benn & Evans, 2014), where ice  
237 flow becomes less constrained, which could explain the origin of the topographic high  
238 we observe at 100 km along profile A-A'. Two smaller topographic highs at 35 km (III;  
239 Fig. 3c) and 45 km (IV; Fig. 3c) along profile A-A' are around 50 m in height, each sep-  
240 arated by deeper basin areas, indicative of ice having been grounded at these points for  
241 some time.

242 A deep central trough punctuated with transverse topographic highs has also been  
243 observed under the neighbouring Fimbul Ice Shelf (Nøst, 2004) and along the adjacent  
244 Coats Land ice margin (Hodgson et al., 2018, 2019). Under the front of Roi Baudouin  
245 Ice Shelf, Eastern DML, an 850 m deep trough (Berger, 2017; Favier et al., 2016) is present,  
246 hinting that this may also extend under the ice shelf in a similar way. This emerging pic-  
247 ture suggests such deep troughs are ubiquitous in this sector of East Antarctica, indi-  
248 cating ice-streams were a prevalent feature in the past and supporting the need for more  
249 widespread sub-ice shelf bathymetry measurements.

### 3.2 Ice-Ocean Interaction

The implications for ice-ocean interactions in the Ekström region, from the newly mapped ice shelf cavity, refine our understanding of the role of DML ice shelves for the Antarctic ice-sheet mass balance. Along this sector of the Antarctic coast, WDW masses are suppressed below the continental shelf break (Heywood et al., 2013) by the prevailing easterly winds in the ‘fresh shelf’ regime (Thompson et al., 2018) that extends from about 20° W to 30° E. The sub-ice shelf CTD profiles (Fig. 4) confirm this, underpinning the relatively low basal melt rate estimates (Neckel et al., 2012) for the Ekström Ice Shelf. Most of the cavity is filled with relatively cold Eastern Shelf Water (ESW) that resides above the WDW along the DML coast (Nøst et al., 2011). In-situ temperatures are close to the surface freezing point around  $-1.9^{\circ}\text{C}$  and practical salinity around 34.4. Only the upper tens of meters of the individual profiles show colder (Fig. 4a), less saline water masses, indicating buoyant outflows of Ice Shelf Water (ISW) in a surface layer near the ice shelf base, that is aligned along common melt water mixing line (Fig. 4b, Gade (1979)) originating from the ESW.

Although the deeper trough beneath the central part of the ice shelf does not cross-cut the continental shelf break, it provides a possible conduit for warmer inflows reaching onto the continental shelf to enter the ice shelf cavity (Fig. 3c, A-A’). Intermittent, warmer near-bottom inflows have been observed across a slightly deeper sill beneath the neighbouring Fimbul Ice Shelf (Hattermann et al., 2012) and a rise of WDW along the DML coast has been suggested as a possible response to future climate change (Hattermann, 2018; Hellmer et al., 2017). In these scenarios, the newly revealed several hundred meters of water depth of the Ekström cavity would support a cavity overturning circulation, where warm near-bottom inflows can propagate undiluted toward the grounding line, rendering Ekström Ice Shelf more vulnerable to warm inflows than implied by previous bathymetric datasets. Our example is also likely to be instructive for many smaller, unmapped ice shelves that have a similar configuration and glacial history along the DML coast and elsewhere.

The presence of extensive ocean cavities beneath Ekström and potentially other DML ice shelves has implications for the susceptibility to local marine ice sheet instability (Morlighem et al., 2020; Ritz et al., 2015), as well as for far field effects through melt induced altering water-mass properties of the westward boundary current. While

282 ice-shelf melt water presently contributes little to the freshening of the ESW (Zhou et  
283 al., 2014), there is growing evidence that basal melting feedbacks play an important role  
284 for the slope front overturning that controls the depth of the thermocline at the shelf break  
285 (e.g. Hattermann, 2018). This regulates the access of warm water to the vast Filchner-  
286 Ronne Ice Shelf in the Southern Weddell Sea (e.g. Hellmer et al., 2017). A correct rep-  
287 resentation of the warm water pathways to the ice shelves upstream of the Filchner Trough  
288 will hence be crucial to quantifying these effects and assessing the uncertainty of model  
289 projections.

290 Locally, our observed seafloor bathymetry suggests a separation of different circu-  
291 lation regimes beneath the ice shelf. While the central part of the cavity seems to be dom-  
292 inated by the trough system; the eastern portion of the ice shelf, adjacent to Atka Bay,  
293 comprises a relatively shallow water column (Figs. 3a and 3c, C-C') that is likely sub-  
294 ject to intense tidal mixing and may be responsible for the vigorous accretion of marine  
295 ice in the area (S. Arndt et al., 2020). The two successive temperature profiles from the  
296 EIS-4 site confirm the existence of a tidally mixed zone in this region. While the EIS-  
297 4b profile shows a similar vertical gradient in temperature to the profiles obtained in the  
298 deeper part of the cavity, the EIS-4i profile has a more homogeneous vertical temper-  
299 ature structure. The EIS-4i profile was taken about 11 hours later than EIS-4b and ac-  
300 cording to the CATS regional tidal model (Padman et al., 2008), a relatively large am-  
301 plitude tidal wave passed the EIS-4 hole location between the two measurements. Hoppmann  
302 et al. (2015) found that platelet ice crystals leave the ice shelf cavity in intermittent pulses  
303 at this location, and similar tidal flushing events may be responsible for mixing larger  
304 volumes of potentially super-cooled ISW in shallower depths, contributing to the platelet  
305 ice formation under the fast ice in Atka Bay that has been identified as a prominent habi-  
306 tat in the sea-ice ecosystem (e.g. Smetacek et al., 1992). A recent study also shows that  
307 propagating tidal waves may play an important role in modulating basal melting near  
308 the ice shelf grounding lines (Sun et al., 2019), further emphasising the need for knowl-  
309 edge of the local cavity shape to assess and interpret the melt rate variability of a given  
310 region.

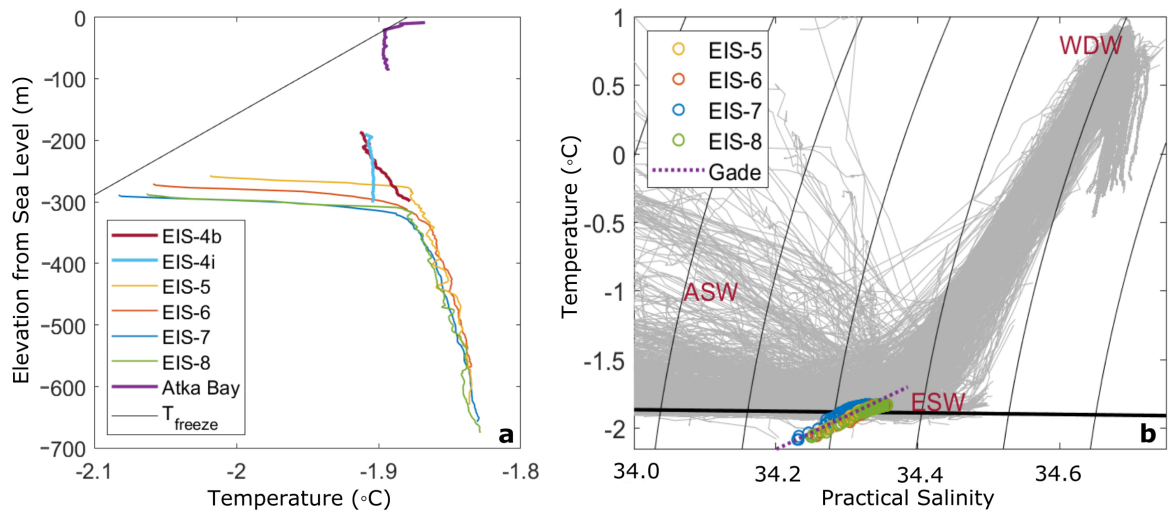


**Figure 4.** Vertical CTD profiles taken through hot-water drilled access holes (4-8; Fig. 3a) and a sea-ice lead (AB; Fig. 3a) **a)** In-situ temperature observed at different sites beneath Ekström Ice Shelf, and beneath sea ice in Atka Bay. Black line indicates the pressure-dependent melting point temperature for a given practical salinity of 34.25. **b)** Distribution of in-situ temperature and practical salinity profiles at the sites where reliable salinity measurements could be obtained. Gray profiles show the regional subset of open ocean CTD profiles presented in Hattermann (2018), indicating ambient water masses with abbreviations indicating the end members of Warm Deep Water (WDW), Eastern Shelf Water (ESW) and Antarctic Surface Water (ASW). The dashed purple line is the melt water mixing line along which a given water mass may transform through interaction with the ice shelf (Gade, 1979) when assuming zero conductive heat flux into the ice. Black curves indicate horizons of constant density, the thick near-horizontal black line indicates the melting point temperature at atmospheric pressure.

## 4 Conclusions

We have presented new bathymetry data from under the Ekström Ice Shelf, Dronning Maud Land, Antarctica. The use of vibroseis seismic reflection surveys proves an effective method for collecting high resolution data across large areas of the ice shelf. As a result, the Ekström Ice Shelf cavity is currently one of the best mapped in Antarctica. The discovery of a deep trough with transverse sills under Ekström Ice Shelf is the second example of such a feature under a DML ice shelf, after the neighbouring Fimbul Ice Shelf, with similar features also found along the adjacent Coats Land margin (Hodgson et al., 2018, 2019) and at the ice-shelf front of Roi Baudouin (Berger, 2017; Favier et al., 2016). This growing list of evidence suggests that the bathymetry we see at Ekström, Fimbul and along the Coats Land coast is likely characteristic of other ice shelves in the DML and neighbouring regions. While these ice shelves are small, they are numerous and very little is known about the cavity geometry, which is a fundamental gap in our ability to understand past ice dynamics and future stability of this region. The ice shelves of DML are known to play a key role in preconditioning the water-mass properties of the westward flowing boundary current, which affects the much larger Filchner-Ronne Ice Shelf and thus large portions of the West Antarctica Ice Sheet. Improved knowledge of ice-shelf cavities is a key required step towards better understanding and projections of the fate of marine ice sheets in a warming climate.

## Acknowledgments

Field work and data processing by ECS since 2016 was funded through the AWI-BGR Sub-EIS-Obs Project. ECS was additionally funded through the DFG Cost S2S project, grant number EI672/10-1 in the framework of the priority programme “Antarctic Research with comparative investigations in Arctic ice areas”, RD by the grant MA 3347/10-1, EH 329/13-1 and DR 822/3-1. The field work of A. Lambrecht in 2010 was kindly supported by the Institute of Meteorology and Geophysics, University of Innsbruck, Austria. SB was partly funded by the MIMO (Monitoring melt where Ice Meets Ocean) project, Belgian Science Policy contract No. SR/00/336. We thank R. Blenkner, J. Köhler, H. Schubert, J. Tell, B. Ehlers, S. Hilmarsson and the staff at Neumayer Station III for logistical and other support. N. Koglin for discussion on hot-water drilled access hole locations and geological constraints. The authors would like to thank C. Haas and J-L. Tison for loan on the CTD equipment, D. Hodgson and one anonymous reviewer for con-

343 structutive and detailed feedback and Emerson E&P Software, Emerson Automation So-  
344 lutions, for providing licenses for the seismic software Paradigm, in the scope of the Emer-  
345 sion Academic Program. The initial idea for envisaging a geologic drilling underneath Ek-  
346 ström Ice Shelf was put forward by Y. Kristoffersen, who's stimulating creativity and  
347 technical support over the years the authors would like to acknowledge in particular. The  
348 gridded bathymetry data and CTD data are archived with PANGAEA (<https://www.pangaea.de/>),  
349 the doi for each data set will be provided on acceptance of the paper.

350 **Author Contributions:** All authors contributed to seismic target and profiling  
351 design, discussed the manuscript and contributed comments towards the final version.  
352 ECS designed and wrote the paper, performed fieldwork and led one field season, anal-  
353 ysed and interpreted seismic data; TH analysed CTD data and provided the oceanographic  
354 component to the paper; DF and A Lambrecht performed seismic data acquisition and  
355 analysis, CM performed seismic data acquisition and led one field season, SB acquired  
356 and analysed CTD data and provided glaciological constrains for ice shelf processes, RD,  
357 TAE and CM contributed ice-flow modelling results and glaciological/geological constraints  
358 for data interpretation, CH was in charge of the seismic equipment and processed seis-  
359 mic data, GK, CG, A Läufer and RT provided geological constraints for data interpre-  
360 tation, FW prepared and coordinated the hot water drilling system, RG led one field sea-  
361 son and performed cavity sampling, OE coordinated and implemented the seismic field  
362 work, led three field seasons, performed seismic and CTD data acquisition. GK, CG, A  
363 Läufer, RT, FW and OE are project Co-PIs, designed financial support and project im-  
364 plementation, CG and OE administratively coordinated the project. The trans-disciplinary  
365 science component is based on Kuhn and Gaedicke (2015).

## 366 **References**

- 367 Arndt, J. E., Schenke, H. W., Jakobsson, M., Nitsche, F. O., Buys, G., Goleby, B.,  
368 ... Wigley, R. (2013). The International Bathymetric Chart of the Southern  
369 Ocean (IBCSO) Version 1.0-A new bathymetric compilation covering circum-  
370 Antarctic waters. *Geophysical Research Letters*, *40*(12), 3111–3117. doi:  
371 10.1002/grl.50413
- 372 Arndt, S., Hoppmann, M., Schmithüsen, H., Fraser, A. D., & Nicolaus, M. (2020).  
373 Seasonal and interannual variability of landfast sea ice in Atka Bay, Wed-  
374 dell Sea, Antarctica. *The Cryosphere Discussions*(January), 1–26. doi:

- 375 <http://doi.org/10.5194/tc-2019-293>
- 376 Benn, D., & Evans, D. J. A. (2014). Erosional Processes, Forms and Landscapes. In  
377 *Glaciers and glaciation* (2nd ed., p. 816). Routledge.
- 378 Berger, S. (2017). *Stability of Antarctic ice shelves - A case study of Roi Baudoin*  
379 *Ice Shelf, Dronning Maud Land, East Antarctica* (PhD). Université Libre De  
380 Bruxelles.
- 381 Cochran, J. R., Jacobs, S. S., Tinto, K. J., & Bell, R. E. (2014). Bathymetric and  
382 oceanic controls on Abbot Ice Shelf thickness and stability. *The Cryosphere*,  
383 *8*(3), 877–889. doi: 10.5194/tc-8-877-2014
- 384 Dupont, T. K., & Alley, R. B. (2005). Assessment of the importance of ice-shelf but-  
385 tressing to ice-sheet flow. *Geophysical Research Letters*, *32*(4), n/a–n/a. doi:  
386 10.1029/2004GL022024
- 387 Eisen, O., Hofstede, C., Diez, A., Kristoffersen, Y., Lambrecht, A., Mayer, C., ...  
388 Hilmarsson, S. (2015). On-ice vibroseis and snowstreamer systems for geoscientific  
389 research. *Polar Science*, *9*(1), 51–65. doi: 10.1016/j.polar.2014.10.003
- 390 Eisermann, H., Eagles, G., Ruppel, A., Smith, E. C., Jokat, W., & Resources, N.  
391 (2020). Bathymetry beneath ice shelves of western Dronning Maud Land ,  
392 East Antarctica , and implications on ice shelf stability. *Geophysical Research*  
393 *Letters (in review)*.
- 394 Fahrbach, E., Rohardt, G., Schröder, M., & Strass, V. (1994). Transport and struc-  
395 ture of the weddell gyre. *Annales Geophysicae*, *12*(9), 840–855. doi: 10.1007/  
396 s00585-994-0840-7
- 397 Favier, L., Pattyn, F., Berger, S., & Drews, R. (2016). Dynamic influence of pin-  
398 ning points on marine ice-sheet stability: A numerical study in Dronning  
399 Maud Land, East Antarctica. *The Cryosphere*, *10*(6), 2623–2635. doi:  
400 10.5194/tc-10-2623-2016
- 401 Förste, C., Schmidt, R., Stubenvoll, R., Flechtner, F., Meyer, U., König, R., ...  
402 Esselborn, S. (2008). The GeoForschungsZentrum Potsdam/Groupe de  
403 Recherche de Géodésie Spatiale satellite-only and combined gravity field mod-  
404 els: EIGEN-GL04S1 and EIGEN-GL04C. *Journal of Geodesy*, *82*(6), 331–346.  
405 doi: 10.1007/s00190-007-0183-8
- 406 Fretwell, P., Pritchard, H. D., Vaughan, D. G., Bamber, J. L., Barrand, N. E.,  
407 Bell, R., ... Zirizzotti, A. (2013). Bedmap2: improved ice bed, surface

- 408 and thickness datasets for Antarctica. *The Cryosphere*, 7(1), 375–393. doi:  
409 10.5194/tc-7-375-2013
- 410 Gade, H. G. (1979). Melting of Ice in Sea Water: A Primitive Model with Applica-  
411 tion to the Antarctic Ice Shelf and Icebergs. *Journal of Physical Oceanography*,  
412 9(1), 189–198. doi: 10.1175/1520-0485(1979)009<0189:MOIISW>2.0.CO;2
- 413 Goldberg, D. N., Gourmelen, N., Kimura, S., Millan, R., & Snow, K. (2019). How  
414 Accurately Should We Model Ice Shelf Melt Rates? *Geophysical Research Let-  
415 ters*, 46(1), 189–199. doi: 10.1029/2018GL080383
- 416 Grobe, H., & Mackensen, A. (1992). Late Quaternary climatic cycles as recorded in  
417 sediments from the Antarctic continental margin. In *Antarctic research series*  
418 (Vol. 56, pp. 349–376). doi: 10.1029/AR056p0349
- 419 Hattermann, T. (2018). Antarctic Thermocline Dynamics along a Narrow Shelf with  
420 Easterly Winds. *Journal of Physical Oceanography*, 48(10), 2419–2443. doi: 10  
421 .1175/JPO-D-18-0064.1
- 422 Hattermann, T., Nøst, O. A., Lilly, J. M., & Smedsrud, L. H. (2012). Two years of  
423 oceanic observations below the Fimbul Ice Shelf, Antarctica. *Geophysical Re-  
424 search Letters*, 39(12), n/a–n/a. doi: 10.1029/2012GL051012
- 425 Hattermann, T., Smedsrud, L. H., Nøst, O. A., Lilly, J. M., & Galton-Fenzi, B. K.  
426 (2014). Eddy-resolving simulations of the Fimbul Ice Shelf cavity circulation:  
427 Basal melting and exchange with open ocean. *Ocean Modelling*, 82, 28–44.  
428 doi: 10.1016/j.ocemod.2014.07.004
- 429 Hellmer, H. H., Kauker, F., Timmermann, R., & Hattermann, T. (2017). The Fate  
430 of the Southern Weddell Sea Continental Shelf in a Warming Climate. *Journal  
431 of Climate*, 30(12), 4337–4350. doi: 10.1175/JCLI-D-16-0420.1
- 432 Heywood, K. J., Locarnini, R. A., Frew, R. D., Dennis, P. F., & King, B. A. (2013,  
433 mar). Transport and Water Masses of the Antarctic Slope Front System in  
434 The Eastern Weddell Sea. In *Antarctic research series* (Vol. 75, pp. 203–  
435 214). Retrieved from <http://doi.wiley.com/10.1029/AR075p0203> doi:  
436 10.1029/AR075p0203
- 437 Hillenbrand, C.-d., Bentley, M. J., Stollendorf, T. D., Hein, A. S., Kuhn, G., Graham,  
438 A. G., ... Sugden, D. E. (2014). Reconstruction of changes in the Weddell Sea  
439 sector of the Antarctic Ice Sheet since the Last Glacial Maximum. *Quaternary  
440 Science Reviews*, 100, 111–136. doi: 10.1016/j.quascirev.2013.07.020

- 441 Hodgson, D. A., Hogan, K., Smith, J. M., Smith, J. A., Hillenbrand, C. D., Gra-  
 442 ham, A. G., . . . Larter, R. (2018). Deglaciation and future stability of the  
 443 Coats Land ice margin, Antarctica. *The Cryosphere*, *12*(7), 2383–2399. doi:  
 444 10.5194/tc-12-2383-2018
- 445 Hodgson, D. A., Jordan, T. A., De Rydt, J., Fretwell, P. T., Seddon, S. A., Becker,  
 446 D., . . . Vaughan, D. G. (2019). Past and future dynamics of the Brunt Ice  
 447 Shelf from seabed bathymetry and ice shelf geometry. *The Cryosphere*, *13*(2),  
 448 545–556. doi: 10.5194/tc-13-545-2019
- 449 Hoppmann, M., Nicolaus, M., Paul, S., Hunkeler, P. A., Heinemann, G., Willmes, S.,  
 450 . . . Gerdes, R. (2015). Ice platelets below Weddell Sea landfast sea ice. *Annals*  
 451 *of Glaciology*, *56*(69), 175–190. doi: 10.3189/2015AoG69A678
- 452 Howat, I. M., Porter, C., Smith, B. E., Noh, M.-J., & Morin, P. (2019). The Refer-  
 453 ence Elevation Model of Antarctica. *The Cryosphere*, *13*(2), 665–674. doi: 10  
 454 .5194/tc-13-665-2019
- 455 IPCC. (2019). *IPCC Special Report on the Ocean and Cryosphere in a Changing*  
 456 *Climate* [H.-O. Pörtner, Roberts, D. C., Masson-Delmotte, V., Zhai, P., Tig-  
 457 nor, M., Poloczanska, E., Mintenbeck, K., Nicolai, M., Okem, A., Petzold, J.  
 458 Rama, B. Weyer, N. (eds.)] (Tech. Rep.). doi: <https://www.ipcc.ch/report/srocc/>
- 459
- 460 Jenkins, A., Dutrieux, P., Jacobs, S. S., McPhail, S. D., Perrett, J. R., Webb, A. T.,  
 461 & White, D. (2010). Observations beneath Pine Island Glacier in West Antarc-  
 462 tica and implications for its retreat. *Nature Geoscience*, *3*(7), 468–472. doi:  
 463 10.1038/ngeo890
- 464 Kobarg. (1988). The tide-dependent dynamics of the Ekstroem Ice Shelf, Antarctica.  
 465 *Berichte zur Polar- und Meeresforschung*, *50*.
- 466 Kristoffersen, Y., Hofstede, C., Diez, A., Blenkner, R., Lambrecht, A., Mayer, C.,  
 467 & Eisen, O. (2014). Reassembling Gondwana: A new high quality constraint  
 468 from vibroseis exploration of the sub-ice shelf geology of the East Antarctic  
 469 continental margin. *Journal of Geophysical Research: Solid Earth*, *119*(12),  
 470 9171–9182. doi: 10.1002/2014JB011479
- 471 Kuhn, G., & Gaedicke, C. (2015). A plan for interdisciplinary process studies and  
 472 geoscientific observations beneath the Eckstroem Ice Shelf (Sub-EIS-Obs). *Po-  
 473 larforschung*, *84*(2), 99–102.

- 474 Meijers, A. J. S., Meredith, M. P., Abrahamsen, E. P., Morales Maqueda, M. A.,  
475 Jones, D. C., & Naveira Garabato, A. C. (2016). Wind-driven export of  
476 Weddell Sea slope water. *Journal of Geophysical Research: Oceans*, *121*(10),  
477 7530–7546. doi: 10.1002/2016JC011757
- 478 Meredith, M. P., Gordon, A. L., Naveira Garabato, A. C., Abrahamsen, E. P., Hu-  
479 ber, B. A., Jullion, L., & Venables, H. J. (2011). Synchronous intensification  
480 and warming of Antarctic Bottom Water outflow from the Weddell Gyre.  
481 *Geophysical Research Letters*, *38*(3), 1–4. doi: 10.1029/2010GL046265
- 482 Milillo, P., Rignot, E., Rizzoli, P., Scheuchl, B., Mouginot, J., Bueso-Bello,  
483 J., & Prats-Iraola, P. (2019). Heterogeneous retreat and ice melt of  
484 Thwaites Glacier, West Antarctica. *Science Advances*, *5*(1), 1–8. doi:  
485 10.1126/sciadv.aau3433
- 486 Morlighem, M., Rignot, E., Binder, T., Blankenship, D., Drews, R., Eagles, G., ...  
487 Young, D. A. (2020). Deep glacial troughs and stabilizing ridges unveiled  
488 beneath the margins of the Antarctic ice sheet. *Nature Geoscience*, *13*(2),  
489 132–137. doi: 10.1038/s41561-019-0510-8
- 490 Neckel, N., Drews, R., Rack, W., & Steinhage, D. (2012). Basal melting at the  
491 Ekström Ice Shelf, Antarctica, estimated from mass flux divergence. *Annals of*  
492 *Glaciology*, *53*(60), 294–302. doi: 10.3189/2012AoG60A167
- 493 Nicholls, K. W., Abrahamsen, E. P., Buck, J. J. H., Dodd, P. A., Goldblatt, C.,  
494 Griffiths, G., ... Wilkinson, J. P. (2006). Measurements beneath an Antarc-  
495 tic ice shelf using an autonomous underwater vehicle. *Geophysical Research*  
496 *Letters*, *33*(8), L08612. doi: 10.1029/2006GL025998
- 497 Nøst, O. A. (2004). Measurements of ice thickness and seabed topography under  
498 the Fimbul Ice Shelf, Dronning Maud Land, Antarctica. *Journal of Geophysi-  
499 cal Research*, *109*(11), 1–14. doi: 10.1029/2004JC002277
- 500 Nøst, O. A., Biuw, M., Tverberg, V., Lydersen, C., Hattermann, T., Zhou, Q., ...  
501 Kovacs, K. M. (2011). Eddy overturning of the Antarctic Slope Front controls  
502 glacial melting in the Eastern Weddell Sea. *Journal of Geophysical Research*,  
503 *116*(11), 1–17. doi: 10.1029/2011JC006965
- 504 Padman, L., Erofeeva, S. Y., & Fricker, H. A. (2008). Improving Antarctic tide mod-  
505 els by assimilation of ICESat laser altimetry over ice shelves. *Geophysical Re-  
506 search Letters*, *35*(22), L22504. doi: 10.1029/2008GL035592

- 507 Paolo, F. S., Fricker, H. A., & Padman, L. (2015). Volume loss from Antarctic ice  
508 shelves is accelerating. *Science*, *348*(6232), 327–331. doi: 10.1126/science  
509 .aaa0940
- 510 Patton, H., Swift, D., Clark, C., Livingstone, S., & Cook, S. (2016). Distribution  
511 and characteristics of overdeepenings beneath the Greenland and Antarctic  
512 ice sheets: Implications for overdeepening origin and evolution. *Quaternary  
513 Science Reviews*, *148*, 128–145. doi: 10.1016/j.quascirev.2016.07.012
- 514 Pattyn, F., Favier, L., Sun, S., & Durand, G. (2017). Progress in Numerical Mod-  
515 eling of Antarctic Ice-Sheet Dynamics. *Current Climate Change Reports*, *3*(3),  
516 174–184. doi: 10.1007/s40641-017-0069-7
- 517 Pritchard, H. D., Ligtenberg, S. R., Fricker, H. A., Vaughan, D. G., Van Den  
518 Broeke, M. R., & Padman, L. (2012). Antarctic ice-sheet loss driven by basal  
519 melting of ice shelves. *Nature*, *484*(7395), 502–505. doi: 10.1038/nature10968
- 520 Rignot, E., Jacobs, S., Mouginot, J., & Scheuchl, B. (2013). Ice-Shelf Melt-  
521 ing Around Antarctica. *Science*, *341*(6143), 266–270. doi: 10.1126/  
522 science.1235798
- 523 Ritz, C., Edwards, T. L., Durand, G., Payne, A. J., Peyaud, V., & Hindmarsh, R. C.  
524 (2015). Potential sea-level rise from Antarctic ice-sheet instability constrained  
525 by observations. *Nature*, *528*(7580), 115–118. doi: 10.1038/nature16147
- 526 Smetacek, V., Scharek, R., Gordon, L. I., Eicken, H., Fahrback, E., Rohardt, G., &  
527 Moore, S. (1992). Early spring phytoplankton blooms in ice platelet layers  
528 of the southern Weddell Sea, Antarctica. *Deep Sea Research Part A, Oceanographic  
529 Research Papers*, *39*(2), 153–168. doi: 10.1016/0198-0149(92)90102-Y
- 530 Sun, S., Hattermann, T., Pattyn, F., Nicholls, K. W., Drews, R., & Berger, S.  
531 (2019). Topographic Shelf Waves Control Seasonal Melting Near Antarctic  
532 Ice Shelf Grounding Lines. *Geophysical Research Letters*, *46*(16), 9824–9832.  
533 doi: 10.1029/2019GL083881
- 534 Thompson, A. F., Stewart, A. L., Spence, P., & Heywood, K. J. (2018). The Antarc-  
535 tic Slope Current in a Changing Climate. *Reviews of Geophysics*, *56*(4), 741–  
536 770. doi: 10.1029/2018RG000624
- 537 Timmermann, R., & Hellmer, H. H. (2013). Southern Ocean warming and increased  
538 ice shelf basal melting in the twenty-first and twenty-second centuries based  
539 on coupled ice-ocean finite-element modelling. *Ocean Dynamics*, *63*(9-10),

- 540 1011–1026. doi: 10.1007/s10236-013-0642-0
- 541 Tinto, K. J., Padman, L., Siddoway, C. S., Springer, S. R., Fricker, H. A., Das, I., . . .  
542 Bell, R. E. (2019). Ross Ice Shelf response to climate driven by the tectonic  
543 imprint on seafloor bathymetry. *Nature Geoscience*, *12*(6), 441–449. doi:  
544 10.1038/s41561-019-0370-2
- 545 Zhou, Q., Hattermann, T., Nøst, O. A., Biuw, M., Kovacs, K. M., & Lydersen, C.  
546 (2014). Wind-driven spreading of fresh surface water beneath ice shelves in  
547 the Eastern Weddell Sea. *Journal of Geophysical Research: Oceans*, *119*(6),  
548 3818–3833. doi: 10.1002/2013JC009556